Catalysis Science & Technology

ROYAL SOCIETY OF CHEMISTRY

PAPER

View Article Online
View Journal | View Issue

Cite this: *Catal. Sci. Technol.*, 2025, 15, 1070

Operando X-ray absorption spectroscopic flow cell for electrochemical CO_2 reduction: new insight into the role of copper species†

Santhosh K. Matam, *[ab] P. K. Sharma, [c] E. H. Yu,*[cd] C. Drivas, [ab] M. D. Khan,[c] M. Wilding,[ab] N. Ramanan,[e] D. Gianolio, [e] M. A. Isaacs, [fg] S. Guan,[h] P. R. Davies [bg] and C. Richard A. Catlow [abf]

We present a novel *operando* X-ray absorption spectroscopic (XAS) flow cell, consisting of a gas chamber for CO_2 and a liquid chamber for the electrolyte, to monitor electrochemical CO_2 reduction (eCO_2R) over a gas diffusion electrode (GDE). The feasibility of the flow cell is demonstrated by collecting XAS data (during eCO_2R over Cu-GDE) in a transmission mode at the Cu K-edge. The dynamic behaviour of copper during eCO_2R is captured by XAS, which is complemented by quasi *in situ* Raman and X-ray photoelectron spectroscopy (XPS). The linear combination analyses (LCA) of the X-ray absorption near edge structure (XANES) indicate that copper oxides are the only species present during the first 20 min of eCO_2R, which was corroborated by complementary Raman and XPS. Significantly, the complementary spectroscopic data suggest that the copper composition in the bulk and on the surface Cu-GDE evolve differently at and above 30 min of eCO_2R. LCA indicates that at 60 min, 77% of copper occurs as metallic Cu and the remaining 23% in the Cu(II) oxidation state, which is not evident from the XPS results that show 100% of the copper is in <2+ oxidation state. Thus, Cu(II) is probably in the bulk of Cu-GDE, as is also evident from Raman spectroscopic result. The ethylene formation correlates very well with the occurrence of copper oxides and hydroxide species in Cu-GDE. The results not only demonstrate the applicability and versatility of the *operando* XAS GDE flow cell, but also illustrate the unique advantages of combining XAS with complementary Raman and XPS that enables the monitoring of the catalyst structural evolution from the bulk to surface and surface-adsorbed species.

Received 9th May 2024,
Accepted 30th November 2024

DOI: 10.1039/d4cy00602j

rsc.li/catalysis

1. Introduction

Electrochemical CO_2 reduction (eCO_2R) over a copper gas diffusion electrode (Cu-GDE) has the potential to generate multi-carbon products (C_{2+}, including ethylene and ethanol) using renewable electricity at a commercial scale,[1–7] and it is necessary to develop the potential and selectivity towards a desired product with acceptable current densities.[1–11] Several studies have attempted to understand the catalyst structure, activity and selectivity relationships by different techniques, with several of these employing *in situ* and/or *operando* spectroscopic techniques.[5,7,12–15] *Operando* spectroscopy is critical as it enables the simultaneous monitoring of the catalyst structure, surface-adsorbed species/reaction pathways and products.[5,12–18] Moreover, a combination of several spectroscopic methods in a single *operando* cell can offer complementary information under identical conditions.[16–19] While *operando* methodologies are routinely applied in the field of heterogeneous catalysis,[16–19] they are still developing in the field of eCO_2R,[5] with some studies reporting *operando* X-ray absorption spectroscopy (XAS) studies of eCO_2R on GDE involving flow cells,[12–14] including zero-gap cells.[15]

A modified GDE flow cell is commonly used to conduct *operando* XAS studies in fluorescence mode, for which a Kapton

[a] *The UK Catalysis Hub, Research Complex at Harwell, Rutherford Appleton Laboratory, Harwell Science and Innovation Campus, OX11 0FA, UK. E-mail: santhosh.matam@rc-harwell.ac.uk*
[b] *Cardiff Catalysis Institute, School of Chemistry, Cardiff University, Cardiff CF10 3AT, UK*
[c] *Department of Chemical Engineering, Loughborough University, Loughborough, LE11 3TU, UK*
[d] *School of Chemistry and Chemical Engineering, University of Southampton, SO17 1BJ, UK. E-mail: eileen.yu@soton.ac.uk*
[e] *Diamond Light Source Ltd., Harwell Science and Innovation Campus, Didcot OX11 0DE, UK*
[f] *Department of Chemistry, University College London, 20 Gordon Street, London WC1H 0AJ, UK*
[g] *HarwellXPS, Research Complex at Harwell, Rutherford Appleton Laboratory, Harwell Science and Innovation Campus, OX11 0FA, UK*
[h] *Maxwell Centre, Cavendish Laboratory, University of Cambridge, JJ Thomson Avenue, Cambridge, CB3 0HE, UK*

† Electronic supplementary information (ESI) available. See DOI: https://doi.org/10.1039/d4cy00602j

window is created at the gas chamber that allows X-rays to penetrate the catalyst surface through the back of the GDE, and all other components of the cell are retained.[12,13] Using this setup, copper (Cu) sputtered on carbon paper[12] or on polytetrafluoroethylene (PTFE)[13] as a working electrode was studied by *operando* XAS during eCO_2R, and it was concluded that Cu is mainly in the metallic state during the reaction. In marked contrast, ref. 13 also demonstrated the gradual conversion of $Cu(OH)_2$ into metallic Cu during 60 min eCO_2R over $Cu(OH)_2$-GDE. A mixture of $Cu(OH)_2$ and metallic Cu was observed at 30 min of eCO_2R, while only metallic Cu was present at 60 min. Moreover, the study reported in ref. 12 finds no clear correlation between the Cu-GDE properties and product selectivity as a function of current density.

Unlike the above two cell designs and experimental conditions,[12,13] an *in situ* grazing incidence (GI) XAS and XRD study[14] that employed a polycrystalline Cu thin film (on a Cr layer-containing Si(100) surface) and CO_2-saturated electrolyte flow concluded that only metallic Cu was present during eCO_2R. In contrast, *operando* XAS studies of KOH-incorporated Cu nanoparticles (Cu-KOH) in a zero-gap flow cell show the presence of metallic Cu, along with a fraction of oxide-derived Cu species (*i.e.*, Cu_2O and $Cu(OH)_2$) during eCO_2R.[15] Thus, the authors attributed the improved ethylene production to the synergistic effect of the Cu_2O and $Cu(OH)_2$ species.

It is evident that there is no consensus on the active and selective site/phase composition of copper for ethylene production. The discrepancies could be a result of varied experimental conditions and *in situ/operando* cell designs.[5,12–15] The latter could play a key role in obtaining reliable structure–activity data.[16–19] These observations emphasise the need for targeted and cell specific *operando* spectroscopic studies to unravel the structure, activity and selectivity relationships.[5] In the present study, we report a novel *operando* XAS GDE flow cell with a three-phase system (*i.e.*, gaseous CO_2, liquid electrolyte and solid catalyst) to conduct experiments in a transmission mode that probes the Cu-GDE from surface to bulk, and provides information on the copper oxidation and coordination states during the reaction. However, as it would not be possible to distinguish between the surface and bulk composition,[5] a complementary surface sensitive quasi *in situ* X-ray photoelectron spectroscopy (XPS) approach is also employed to probe the copper dynamics on the Cu-GDE surface.[10,20,21] These data are then complemented by Raman spectroscopy measurements that monitor not only the surface adsorbed species, but also the evolution of copper speciation (even very amorphous species) during the reaction.[5,22] On this basis, we derive reliable catalyst structure–activity-selectivity relationships of Cu-GDE during the complex eCO_2R reaction.

2. Materials and methods

2.1 Preparation of the copper gas diffusion electrode (Cu-GDE)

The Cu-GDE preparation is similar to a procedure reported elsewhere.[20] Commercial gas diffusion layer (GDL) and Cu_2O nanoparticles were purchased from Freudenberg (H2315 I2 C6) and EPRUI Nanoparticles & Microspheres Co. Ltd., respectively. 15 mg of Cu_2O nanoparticles were dispersed in 200 μL of isopropanol (99.5%, Sigma-Aldrich) and sonicated for 10 min. Subsequently, 33 μL of 5 wt% Nafion binder (Sigma-Aldrich) was added and the suspension was sonicated for another 60 min. The resulting catalyst ink was then painted layer-by-layer onto the 2 cm^2 surface of GDL. Between each layer, the GDL was subjected to drying at 50 °C for 2 min. The procedure was repeated until a desired catalyst loading of 5 mg cm^{-2} was achieved. The final Cu-GDE was dried at 50 °C for 30 min.

2.2 Characterisation

The phase composition of the as-purchased commercial Cu_2O nanoparticles and the fresh (*i.e.*, the as-prepared final) Cu-GDE is evaluated by X-ray diffraction (XRD) using a Bruker D2 phaser benchtop diffractometer equipped with a Cu Kα radiation source (λ = 1.5406 Å) with a 2θ range of 15–80°. The corresponding data are presented in Fig. S1 of the ESI.†

2.3 Electrochemical CO_2 reduction (eCO_2R)

The eCO_2R experiments were conducted in a standard three-chamber GDE flow cell, which was operated in a three-electrode configuration. The details of the GDE flow reactor are reported elsewhere.[10] Briefly, the cell consists of Cu-GDE as a working electrode, Pt nanoparticles-coated Ti mesh as a counter electrode, and Hg/HgO (RE-5B, BASI, 1 M KOH, 0.118 V *vs.* RHE) as a reference electrode. 1 M KOH was used as the catholyte and anolyte. To prevent the cross-over of liquid products, the catholyte and anolyte chambers were separated by a cation exchange membrane (F-1050, Fumapem). The GDE flow reactor was operated in continuous flow mode by connecting the reactor to the 1 M KOH electrolyte reservoir and to a pure CO_2 gas (20 mL min^{-1}, controlled by a Bronkhorst digital mass flow controller) cylinder (99.9995% purity, BOC). The former enables the collection of liquid products at a regular interval. Gas phase and alcoholic liquid products were analysed by a gas chromatography (Shimadzu Tracera GC-2010) instrument equipped with a barrier discharge ionization detector (BID). The ShinCarbon ST micropacked column 80/100 (Restek) was used to quantify the permanent gases and light hydrocarbons, while the Zebron ZB-WAXplus capillary column (Phenomenex) was used to quantify alcoholic liquids. An ion chromatography (Eco IC, Metrohm) instrument equipped with a Metrohm 6.1005.200 column was used to quantify volatile fatty acids, including formic acid. A cylinder (BOC) with a customised calibration mixture of H_2 (1.000%), CO (1.000%), CO_2 (96.000%), CH_4 (0.500%), C_2H_4 (0.500%), C_2H_6 (0.500%) and C_3H_6 (0.500%) was used to quantify the gas phase products by an area normalization method. Liquid products were quantified by an external standard method.[20]

The potentials were reported *vs.* reversible hydrogen electrode (RHE), and the current densities were determined based on the GDE surface area of 2 cm^2.[20] The current densities were described as the cathodic current density, and

without any negative sign. The absolute faradaic efficiencies (FE) for each product was calculated based on Faraday's law.[10,20] Liquid products were accumulated continuously and collected for 30 min reaction time, and the absolute FEs of liquid products represented average values. Differently, the gas products were collected during a short period of time in the very last minute of the 30 minute reaction, and the absolute FEs of gas products represented instantaneous values.

2.4 *Operando* XAS GDE cell design and fabrication

The *operando* cell consists of a gas chamber and a liquid chamber made with a Perspex material, and the chambers were separated by a working electrode (*i.e.*, cathode) in contact with the electrolyte. The counter electrode (Pt nanoparticles-coated Ti mesh) was placed in the electrolyte (*i.e.*, anode), and the cell includes a slot for a reference electrode. The cell design is a simplified version of the standard three chamber electrochemical cell, as described above in section 2.3, and as reported in ref. 10. The computer aided design (CAD) of the *operando* cell is shown in Fig. 1. The gas chamber is sealed off with a Kapton window that faces the oncoming X-ray beam. Gaseous CO_2 enters through the gas chamber, and then diffuses through the porous GDE on to the catalyst surface. The unreacted CO_2 and gas phase products mostly diffuse back through the GDE, and exit through the gas chamber *via* an outlet that can be connected to a mass spectrometry (MS). Meanwhile, liquid products exit through the aqueous electrolyte, which can be continuously circulated and can be collected for analyses. The liquid chamber is also sealed off with a Kapton window such that the X-ray beam passes through it to the detector, and the X-ray beam probes both working electrode and electrolyte. Therefore, the cell is especially suitable for experiments in a transmission mode, but can also be used for measurements in a fluorescence mode. Moreover, the cell can be coupled with another technique, such as XRD or vibrational spectroscopy (for example Raman).

The eCO_2R experiments were conducted using the *operando* XAS GDE flow cell to assess the effect of the cell design on the product distribution, as compared to the standard GDE flow cell. Similar experimental conditions were employed, as described in section 2.3. The *operando* cell was operated in a galvanostatic mode at 400 mA. Potentials were measured, which were in a range between 2.2 and 2.7 V, comparable to the standard cell. The *operando* cell was operated in a continuous flow mode by connecting the reactor to the 1 M KOH electrolyte reservoir and to a pure CO_2 gas (20 mL min^{-1}) cylinder (BOC). The products and unreacted CO_2 were analysed and quantified according to the procedure described in section 2.3.[10,20]

2.5 *In situ* XAS

In situ XAS experiments were conducted at the B18 beamline of the Diamond Light Source (DLS), UK. A photograph of the cell setup on the B18 beamline is shown in the inset of Fig. 1. XAS measurements were conducted at the Cu K-edge in a transmission mode using the quick EXAFS (QEXAFS) setup with a fast-scanning Si(111) double crystal monochromator.[23] A set of Pt-coated mirrors was used to reject higher harmonics from the X-ray beam. Ionization chambers filled with appropriate gas mixtures were used to

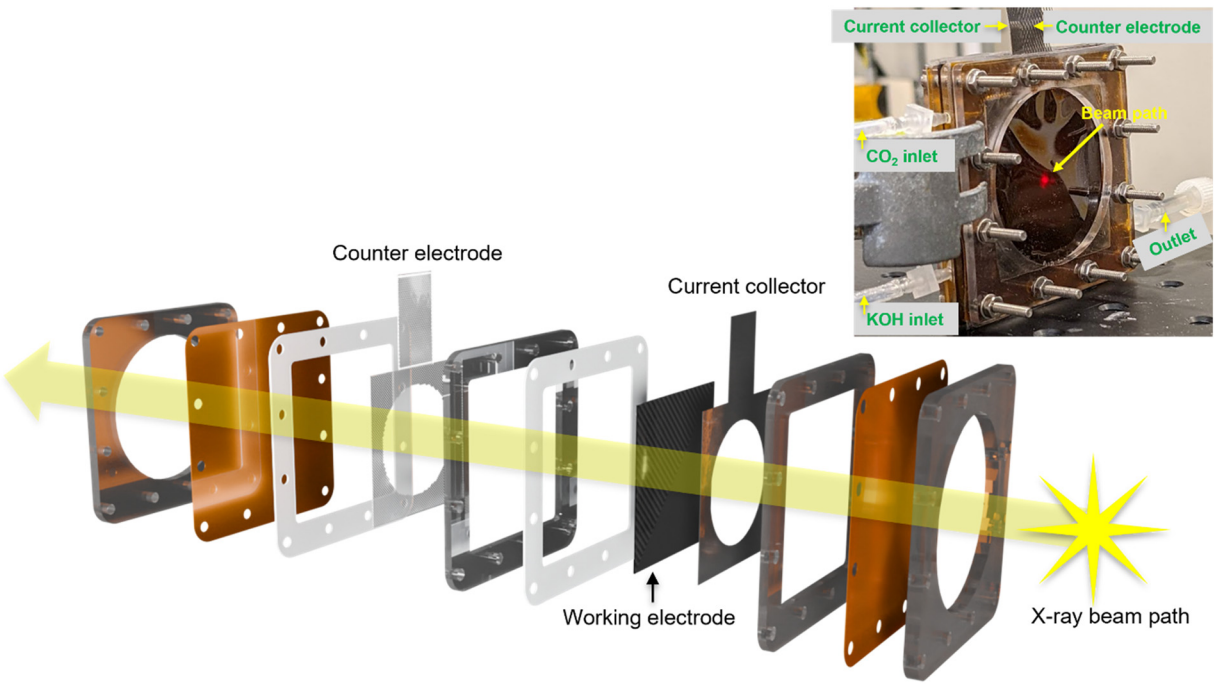

Fig. 1 CAD image of the *operando* XAS-GDE flow cell. The inset photograph shows the cell setup on the beamline.

measure the incident beam intensity, I_0, the transmitted beam through the Cu-GDE, I_t, and through the reference, I_{ref}. A standard Cu foil reference was placed between I_t and I_{ref}. The X-ray beam passes through the centre of the working Cu-GDE, which is indicated by a red laser spot (see the inset of Fig. 1). *In situ* XAS data were collected during the eCO_2R reaction at different time intervals; at 0.5, 10, 20, 30 and 60 min. The eCO_2R reaction conditions were identical to those described in section 2.3 for the *operando* XAS GDE flow cell.

The raw XAS spectra were processed using the software Athena.[24] The spectra were pre-edge subtracted and normalised to the post-edge background. The linear combination analyses (LCA) of the normalised X-ray absorption near edge structure (XANES) spectra were then performed around the Cu K-edge using the software Athena.[24] The XANES spectra of the reference samples Cu metal foil, Cu_2O, CuO, $CuCl_2{\cdot}2H_2O$ and $Cu_4(OH)_6Cl_2$ were used as standards for the LCA. Their weights were constrained to be between 0 and 1, and their sum to be equal to 1. The initial selection of standard spectra for LCA analyses is determined based on the materials used for the preparation of Cu-GDE and characterisation results, and unknown Cu species were modelled with reference to copper chloride compounds to obtain a best possible fit.

2.6 Quasi *in situ* Raman spectroscopy

For quasi *in situ* studies, a series of eCO_2R experiments were conducted in a nitrogen glove box using a standard GDE flow cell, as described in section 2.3, and the Cu-GDE samples were studied at different time intervals between 0 and 60 min. At each time point, a fresh Cu-GDE was used. The as-collected samples were then loaded on to a Thermo Fisher vacuum transfer stage within the glovebox, and then the samples were transferred for Raman spectroscopy measurements. Raman data were acquired using a Thermo iXR coincident Raman spectrometer mounted inside a Thermo NEXSA XPS spectrometer. All measurements were taken using a 455 nm laser, a step size of 0.1 cm^{-1} and a dwell time of 20 seconds.

2.7 Quasi *in situ* X-ray photoelectron spectroscopy (XPS)

As described for quasi *in situ* Raman (section 2.6), a series of Cu-GDE samples at different time intervals of the reaction were prepared. The samples were then transferred using a sealed shuttle holder, and opened in the analysis chamber using a wobble stick. The XPS data were acquired with a Kratos Axis SUPRA using monochromated Al Kα (1486.69 eV) X-rays at 15 mA emission and 15 kV HT (225 W), and a spot size/analysis area of 700 × 300 μm. The instrument was calibrated to gold metal (Au 4f of 83.95 eV), and the dispersion was adjusted to give a binding energy (BE) of 932.6 eV for the Cu $2p_{3/2}$ line of metallic copper. The source resolution for monochromatic Al Kα X-rays is ~0.3 eV. The instrumental resolution was determined to be 0.29 eV at 10 eV pass energy using the Fermi edge of the valence band for metallic silver. Instrument resolution with the charge compensation system on was determined to be <1.33 eV FWHM on PTFE. High-resolution spectra were obtained using a pass energy of 20 eV, step size of 0.1 eV and sweep time of 60 s, resulting in a line width of 0.696 eV for Au $4f_{7/2}$. Survey spectra were obtained using a pass energy of 80 eV. Charge neutralisation was achieved using an electron flood gun with filament current = 0.38 A, charge balance = 2 V, and filament bias = 4.2 V. Spectra have been charge corrected using reference values for the Cu oxides (933.1 and 932.2 eV, respectively, for CuO and Cu_2O), instead of the more usual carbon reference point due to the presence of multiple species attributable to the GDE. All data were recorded at a base pressure of below 9×10^{-9} Torr and a room temperature of 294 K. Data were analysed using CasaXPS v2.3.26rev1.2V.[25] Peaks were fitted with a Shirley background prior to component analyses.

3. Results and discussion

3.1 eCO_2R over Cu-GDE using a standard GDE flow cell

To assess the Cu-GDE efficiency in eCO_2R, a benchmark test is conducted using a standard GDE flow cell.[10] The normalised faradaic efficiency (FE) of gaseous products (C_2H_4, CO and H_2) and the sum of all liquid products is plotted as a function of the reaction time in Fig. 2.

It is evident that the formation of gaseous products within the first 60 min of the reaction is almost stable with FE of 13%, 28% and 22.50% for C_2H_4, CO and H_2, respectively. The FE of C_2H_4 and CO continues to be in steady state for up to 90 min, while the FE of the H_2 evolution increases from 22.5% to 25% in the time period between 60 and 120 min. In contrast, the FE of the liquid products decreases continuously from 37.5% to 32.5% during the reaction time period between 0 and 120 min. The FE of the liquid products decreases dramatically while that of the H_2 evolution increases rapidly above 120 min, indicating the flooding of the cell.[2,10,20] Over the duration of 240 min of the reaction, the current density of the system decreases gradually from 102 to 82 mA cm^{-2}, suggesting a gradual decrease in either catalyst or cell efficiency or both. The reduced cell efficiency can be due to flooding of the GDE, especially after 120 min of the reaction, while the catalyst efficiency during the reaction is a topic of debate.[5,12–15] Both effects are entwined and cannot be decoupled.

3.2 eCO_2R over Cu-GDE using the operando XAS GDE flow cell

The Cu-GDE efficiency in eCO_2R is tested in the *operando* XAS GDE flow cell to verify its performance against the standard cell (Fig. 2). The FE of gaseous products C_2H_4, CO and H_2 as a function of time is shown in Fig. 3. The steady-state formation of gaseous products within the first 60 min of the reaction is evident with FE of 22.5%, 10% and 17% for C_2H_4, CO and H_2, respectively. The formation trend is consistent with the data obtained on the standard cell (Fig. 2), confirming that the *operando* cell design and Cu-GDE efficiency are optimal.

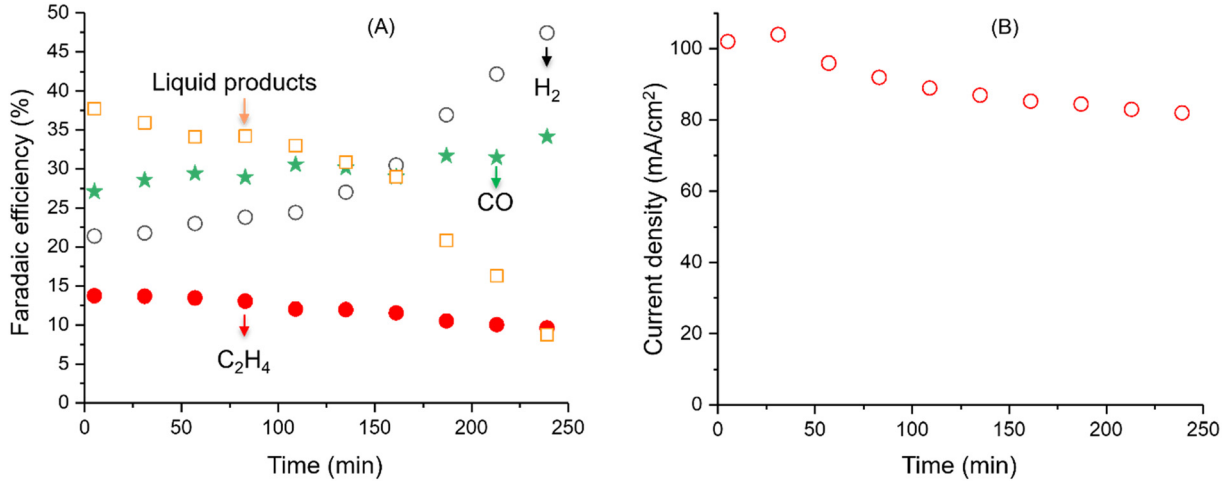

Fig. 2 Normalised FE (%) of products (A) and current density (B) as a function of time. The liquid products are formate, methanol, ethanol and isopropanol. Refer to experimental section 2.3 for details.

We note that the H_2 evolution is gradually increasing with time but it is faster above 60 min, which indicates the flooding of the cell. This is in line with the data reported in Fig. 2. Therefore, the catalyst structure activity studies are conducted within the first 60 min of the reaction, during which a steady state formation of gas phase products is observed. It should also be noted that the slight variations in the FE of the products can be attributed to the simplified *operando* cell configuration (Fig. 1), as compared to the standard GDE flow cell.[10]

3.3 *In situ* XAS

In situ X-ray absorption near edge structure (XANES) spectra collected during the eCO_2R reaction over Cu-GDE are presented along with reference samples in Fig. 4. The three reference samples exhibit unique spectroscopic features, including pre-edge features, edge position and edge features, implying that the oxidation and coordination states of copper in those reference samples are distinctive.[26,27] The edge position of the XANES depends on the oxidation state of the copper species, with the edge position of the metallic Cu being at a lower energy than that of copper oxides.[13,26,27] Likewise, a sharp feature on the rising edge between 8980 and 8986 eV (Fig. 4A) indicates the coordination states of cuprous oxide (Cu_2O) in linear geometry or cupric oxide (CuO) in square planar geometry.[26–28] A similar feature on the rising edge (at 8980 eV) is also typical for metallic Cu with an fcc structure[27–29] that exhibits a characteristic doublet (*i.e.*, two peaks) on the white line at 8993 and 9002 eV (Fig. 4A). Variations in the intensities of the peaks above the white line (at 9002 and 9025 eV) reflect a degree of scattering from the second coordination shell. Hence, they can provide information on the extent of local ordering, which is related to the metal particle size.[27–29] Moreover, the white line intensity appears to be higher for Cu in a higher coordination state than with lower coordination.[26,27,30,31] Accordingly, the white line intensity is higher for Cu in the planar geometry than in the linear geometry (Fig. 4A).

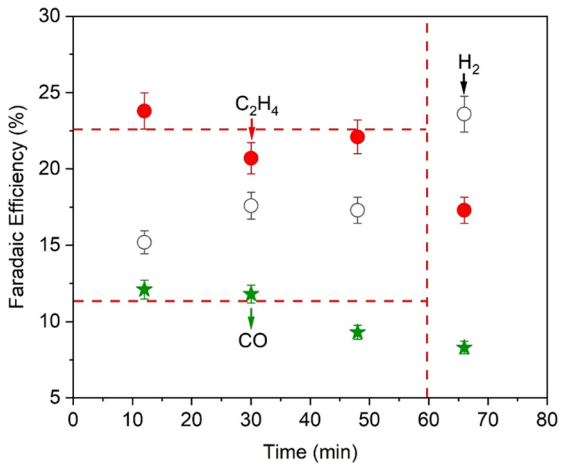

Fig. 3 eCO_2R over the *operando* XAS-Cu-GDE flow cell: the FE (%) of gaseous products are plotted as a function of time. Vertical and horizontal dashed lines are included for guidance purposes. Refer to experimental section 2.4 for details.

In situ XANES at different times of the eCO_2R reaction are shown in Fig. 4B. By visual inspection of the spectra, it appears that copper is in the oxidised state as a mixture of cupric and cuprous oxides within the first 20 min of the reaction; as the edge position, edge features and the pre-edge features are similar to the reference samples CuO and Cu_2O. Within the same period, it is also evident that the intensity of the white line decreases and the sharp feature on the rising edge increases (Fig. 4B inset). These changes imply a decreased coordination state of the copper from planar to linear, and a change in its oxidation state from Cu(II) to Cu(I).[26–28] At 30 min of the reaction, the intensity of the white line decreases further and the sharp feature on the rising edge increases in intensity (Fig. 4B inset). Thus,

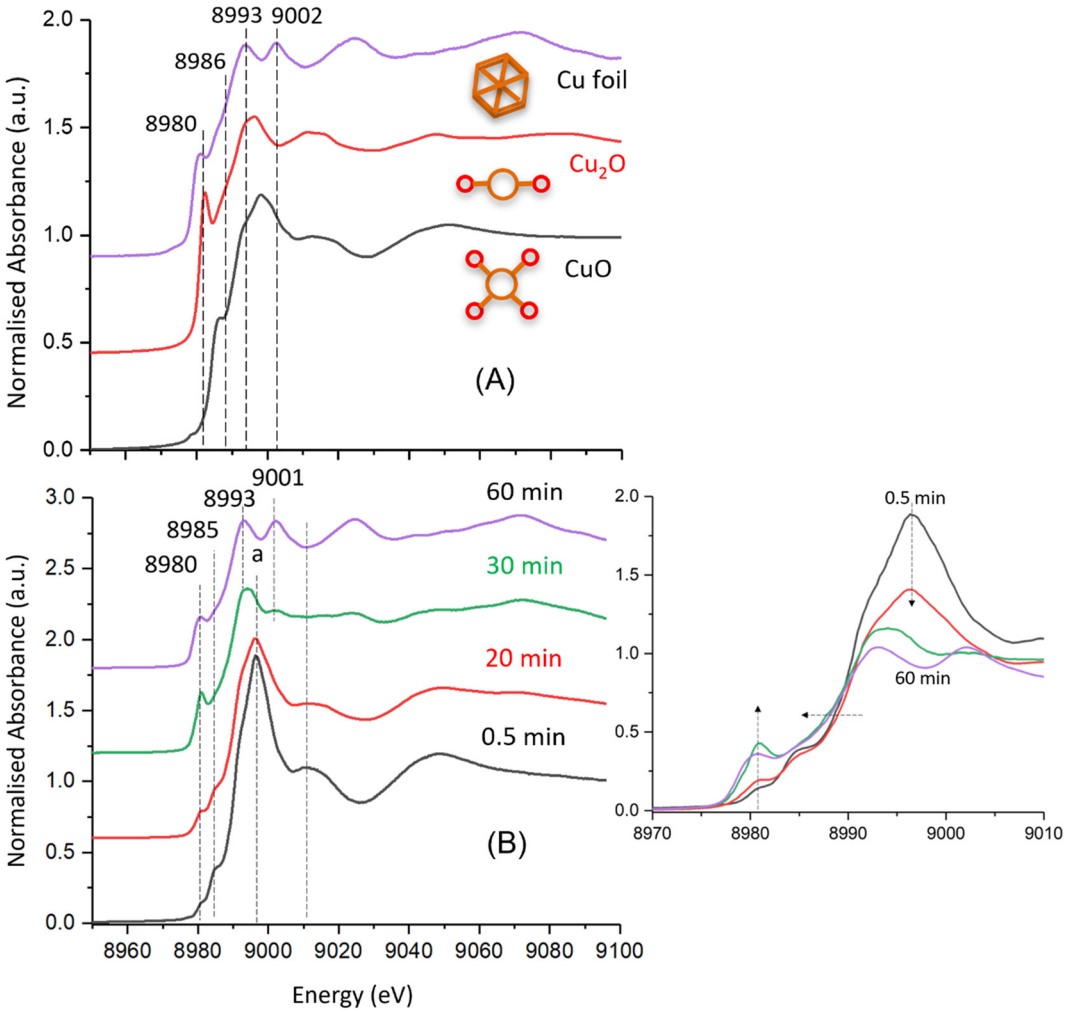

Fig. 4 XANES spectra of reference copper samples (A) and *in situ* XANES spectra of Cu-GDE during the eCO_2R reaction (B). 'a' in the panel (B) indicates the white line of the XANES spectra collected within 20 min, and the inset of the panel (B) shows the overlayed and magnified region of the *in situ* XANES spectra for better visibility of the changes. Refer to experimental sections 2.4 and 2.5 for details. The vertical dashed lines in panels (A) and (B) indicate the energies of the pre-edge features, edge position and edge features. The arrows in the inset of the panel (B) indicate the change in intensities of the features and edge position.

the spectrum now appears to be a mixture of copper oxides and metallic copper (Fig. 4B). The intensities of the peaks at 8996 eV and above the white line at 9012 eV are attenuated, while there are weak features at 9002 and 9025 eV attributable to metallic Cu appear, indicating that the scattering from the second coordination shell is weak.[27–29] These dynamic changes point to the transition of copper oxide to metallic Cu during the reaction. The transition appears to have led to a poorly ordered local environment of copper during the reaction at 30 min. At 60 min of the reaction, the XANES spectrum resembles the reference metallic Cu spectrum (comparison of Fig. 4A and B). This indicates that the transition of the copper oxide phase into metallic Cu is complete, and that the majority of copper now appears to be in the metallic state. The dynamic behaviour of copper is further evaluated, and the evolution of different copper species during the reaction is quantified by linear combination analyses (LCA) of the *in situ* XANES spectra. The corresponding data are shown in Fig. S2† and in Table 1.

LCA indicates the presence of only oxidic copper and no detectable metallic Cu within the first 20 min of the reaction (Fig. S2† and Table 1), as expected from the XANES spectra presented in Fig. 4B. The majority of the oxidic copper is in the Cu(II) oxidation state (82%), while a minority is in the Cu(I) (18%) oxidation state. It appears that a fraction of Cu(II) is in an octahedral coordination state, which is different from the initial CuO phase in planar geometry. The higher coordination state of copper is not surprising under these reaction conditions involving the aqueous electrolyte, reactant and products that interact with the copper, and hence increase the copper coordination number. The presence of Cu(II) in an octahedral coordination state is consistent with the observed higher white line intensity of the XANES spectra, as discussed above (Fig. 4B inset). These observations are consistent with reports that show the

Table 1 Copper composition derived by LCA of *in situ* XANES spectra (Fig. 4B)

eCO_2R time (min)	Contribution of model compounds composition (%) to experimental data				
	Metallic Cu^0	Cu_2O	CuO	$Cu_4(OH)_6Cl_2$	$CuCl_2{\cdot}2H_2O$
20	—	18.3	63.5	18.2	—
30	44	44	12	—	—
60	77	—	—	—	23

presence of copper hydroxide and/or Cu_2O,[13,15] but differ from the proposal that only metallic Cu is present during the reaction, irrespective of the duration.[12–15] The similarities[13,15] and differences[12–15] seem to relate directly to the nature of the initial Cu-GDE composition and experimental conditions.

The LCA of the XANES spectrum collected at 30 min of the reaction shows that the majority of Cu(II) is converted into Cu(I) and metallic Cu (Table 1), and a complex mixture of Cu(II), Cu(I) and metallic Cu occurs, which is also reflected in the salient features of the XANES spectrum displayed in Fig. 4B. These observations are in line with that of $Cu(OH)_2$-GDE studied by *operando* XAS.[13] The metallic Cu content in the Cu-GDE increases to 77% at 60 min of the reaction, as is evident from the LCA (Table 1). However, remarkably, 23% of the copper is in the Cu(II) oxidation state, which is not obvious from the XANES spectrum presented in Fig. 4B, demonstrating the importance of LCA to obtain insights into the copper speciation during the reaction. Interestingly, it appears that the proportion of Cu(II) increases with the reaction time from 30 to 60 min, suggesting continuous evolution and interconversion of the copper species, under these experimental conditions. Our results indicate the presence of a significant proportion of Cu(II), either in the subsurface or bulk of Cu-GDE, which could not be distinguished by XANES during the reaction (especially at 60 min of the reaction when metallic Cu dominates the bulk of the Cu-GDE), aligning well with theoretical studies that predicted an improved C_{2+} production in the presence of subsurface copper oxides.[32,33] It should be noted that the LCA method provides only an indicative information on the copper speciation. Therefore, we have conducted complementary quasi *in situ* Raman and XPS spectroscopic studies under similar conditions. Raman spectroscopy is sensitive to the amorphous phases of the copper species even in the bulk of the Cu-GDE, providing absolute information on the copper speciation and the surface adsorbed species. Meanwhile, XPS is a surface sensitive technique that provides information on the chemical composition and states of copper. Together with Raman and XPS, we aim to further refine the LCA data, and to define the active and selective copper species for the eCO_2 reaction.

3.4 Quasi *in situ* Raman

Quasi *in situ* Raman spectra were collected between 0 and 60 min of the eCO_2R reaction, as shown in Fig. 5.

The Raman spectrum of the fresh Cu-GDE (at time zero of the reaction) shows bands attributable to Cu_2O and CuO,[34–38] consistent with XRD (Fig. S1†) and *in situ* XANES that also indicate no detectable metallic Cu (Fig. 4B and Table 1). Within the first 10 min of the reaction, a band at 490 cm^{-1} appears, along with another band at 295 cm^{-1} that overlaps with CuO. This indicates the formation of a $Cu(OH)_2$ phase during the reaction,[34–37] which is expected under reaction conditions involving direct contact of Cu-GDE with the aqueous electrolyte, reactants and products. $Cu(OH)_2$ is known to adsorb and react with CO_2 even under ambient conditions, though very slowly.[38,39] Hence, it can be anticipated that the hydroxide phase participates in the eCO_2R reaction.[13,40] The occurrence of the hydroxide phase rationalises the LCA of *in situ* XANES that points to the presence of octahedrally coordinated Cu(II) complexes with either water or hydroxides being one of the ligands (Table 1). Therefore, the Cu(II) complexes could be the $Cu(OH)_2$ phase as identified by Raman, demonstrating the critical role of complementarity of the two techniques to draw crucial insights into the complex copper speciation during the reaction. The Cu_2O, CuO and $Cu(OH)_2$ phases persist during the reaction, as is evident from the Raman spectrum collected at 60 min. We note that the presence of these three phases is not obvious from the LCA of *in situ* XANES (Fig. 4B and Table 1), indicating that these species are very amorphous in nature. Thus, the Raman data is critical in identifying real copper oxide and hydroxide phases that occur during the reaction and in deriving catalyst structure activity relationships. A band at 1920 cm^{-1} appears at 60 min, and can be attributed to CO adsorbed on metallic Cu.[34,35] This is in line with XANES that shows a well-established metallic Cu phase at 60 min. The vibrational frequency of the adsorbed CO indicates a bridge bound geometry that is typically observed for large metal

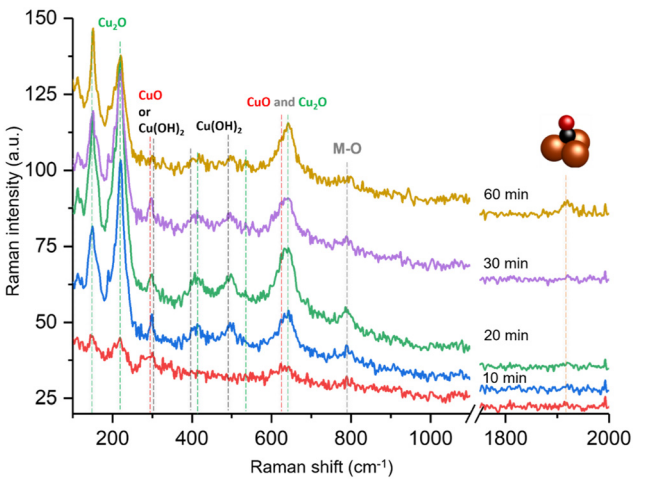

Fig. 5 Quasi *in situ* Raman spectra collected during the eCO_2R reaction. General peak assignments are indicated by the dashed lines. M–O indicates the copper–oxygen bond. Bridge bound CO adsorption on metallic Cu at 1920 cm^{-1} is depicted. Refer to experimental sections 2.3 and 2.6 for details.

particles, consistent with previous studies that reported on the agglomeration of Cu particles during the eCO_2R reaction.[1,15,20,41,42]

3.5 Quasi *in situ* XPS

XPS is a surface sensitive technique; therefore, the evolution of the surface copper composition during the eCO_2R reaction complements the information obtained by XANES and Raman spectroscopy on the bulk composition.[10,20,21] Quantitative data on the copper speciation during the reaction were obtained by deconvolution of the Cu $2p_{3/2}$ peaks of the XPS spectra using the parameters described by Beisinger.[43] The corresponding spectra are depicted in Fig. 6, and the quantitative data are shown in Table 2. Fitting parameters are described in ESI† (Table S1), and detailed fitting is shown in Fig. S3.†

The XPS spectrum of the fresh Cu-GDE at time zero shows two prominent Cu $2p_{3/2}$ peaks between 930 and 945 eV.[10,20,43] The peaks centered at 942 eV are ascribed to the shake-up satellites of the Cu(II), as they are not present for Cu(I) or metallic Cu^0, corroborating the XRD (Fig. S1†), XANES (Fig. 4B), and Raman data (Fig. 5). However, a peak at 932.2 eV indicates the presence of a fraction of either Cu(I) or Cu^0 (shown with green peak fitting). The binding energies of Cu(I) and Cu^0 are very similar ($\Delta_{BE} \approx 0.4$ eV). Hence, it is difficult to distinguish between these two species by XPS.[10,20,21,43] Based on XRD and *in situ* XANES data that show the presence of CuO and Cu_2O, and the absence of metallic Cu, the XPS peak at 932.2 eV can be tentatively assigned to Cu(I) rather than Cu^0. However, the sensitivity of the three techniques is indeed different. Hence, the presence of a fraction of metallic Cu on the Cu-GDE surface cannot be ruled out.[21,43]

Table 2 Copper composition during the eCO_2R reaction derived by deconvolution of the Cu $2p_{3/2}$ peak fitting of quasi *in situ* XPS spectra, reported in Fig. 6

Spectra collected during the reaction at time (min)	Copper composition (%)	
	Cu_2O and/or Cu^0	CuO
0	9	91
10	13	87
20	20	80
30	30	70
60	≈100	0

The quantitative data (Table 2) suggest that CuO dominates the surface composition of the fresh Cu-GDE, which is in good agreement with the bulk composition, as is evident from the *in situ* XANES (Fig. 4B and Table 1) and Raman data (Fig. 5). The XPS and quantitative data derived from the Cu $2p_{3/2}$ peak fitting show that the surface composition evolves during the reaction in the time period between 0 and 60 min (Fig. 6 and Table 2). The intensities of

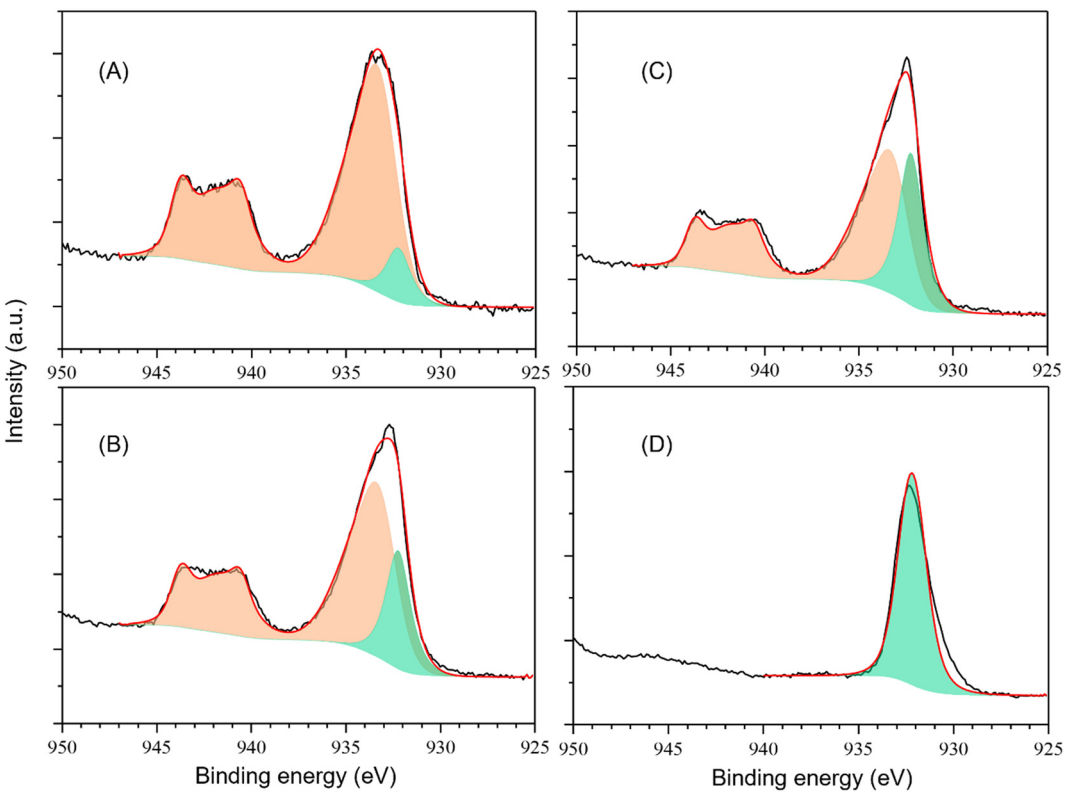

Fig. 6 High-resolution quasi *in situ* XPS spectra, including peak fitting, of Cu 2p of Cu-GDE during the reaction: the Cu-GDE at time 0 (A), 20 (B), 30 (C) and 60 (D) min. Refer to experimental sections (2.3 and 2.7) for details. The sum of the components of each oxidation state, Cu(II) with orange and Cu(I)/Cu(0) with green, is presented for clarity.

the Cu $2p_{3/2}$ peaks change during the reaction. The peaks centred at 933 and 942 eV decrease, while the one at 932.2 eV increases (Fig. 6). At 20 min of the eCO_2R reaction, 80% copper is in the Cu(II) oxidation state and the remaining 20% is in either Cu(I) or Cu^0 oxidation, in excellent agreement with LCA (Table 1). Even at 30 min, 70% copper is still in Cu(II) and the remaining 30% is in a lower oxidation state than Cu(II). The latter could be due to the occurrence of both Cu(I) and Cu^0, as evident from the LCA of *in situ* XANES data (Table 1). We note that the surface composition appears to evolve differently from the bulk at 30 min, as evident from the quantitative data derived from XPS and XANES (Tables 2 and 1, respectively). Accordingly, the surface composition is dominated by Cu(II), while it is in the minority in the bulk. This observation gains further strength at 60 min of the reaction as evident from the disappearance of the Cu(II) peaks (Fig. 6), while a sole peak attributable to either Cu(I) or Cu^0 occurs (Fig. 6 and Table 2). The disappearance of the Cu(II) peak infers complete reduction of surface CuO on the Cu-GDE. In contrast, the LCA of *in situ* XANES data points to the presence of 23% Cu(II) species in the bulk composition of the Cu-GDE (Table 1), and Raman data show the occurrence of Cu(II) O, Cu_2O and $Cu(OH)_2$ phases (Fig. 5) even at 60 min of the reaction, confirming that the bulk composition is indeed different from that of the surface. These observations further demonstrate that the powerful combination of complementary techniques is essential to unravel the structure activity relationships of complex catalytic systems, such as the three phase (*i.e.*, solid–gas–liquid) eCO_2R reaction over Cu-GDE.

4. Structure–activity relationships

Our combination of complementary techniques has allowed us to assess the evolution of the surface and bulk composition of Cu-GDE during the eCO_2R reaction. In summary, it is evident that CuO and Cu_2O occur on the fresh Cu-GDE with no detectable metallic Cu. At 20 min of eCO_2R, the LCA of XANES indicates the occurrence of ≈82% of CuO and ≈18% of Cu_2O (Table 1). This is consistent with the XPS results, which show the presence of 80% CuO and 20% copper in oxidation states less than Cu(II) (Table 2), potentially in the form of Cu(I). The Raman data corroborate the XANES and XPS, and confirms the presence of the CuO and Cu_2O phases on the fresh Cu-GDE (Fig. 5), which is also in agreement with XRD (Fig. S1†). These two copper oxide species persist and a new $Cu(OH)_2$ species appears during the first 20 min of the eCO_2R reaction, as evident from the Raman data presented in Fig. 5. The results are in line with a study that reported the occurrence of ≈95% $Cu(OH)_2$ and the remaining ≈5% as Cu_2O in the fresh $Cu(OH)_2$-GDE.[13] The absolute amounts and speciation reported in[13] differ from our results (Table 1), which can be attributed to the initial composition of the Cu-GDE. The ethylene production within the first 20 min of the eCO_2R reaction (Fig. 2 and 3) is therefore unambiguously attributed to copper oxides and $Cu(OH)_2$ species.

The conversion of copper oxides appears at 30 min of the eCO_2R reaction, as detected by XANES (Fig. 4). The LCA suggests that the majority of CuO is now transformed into Cu_2O and metallic Cu; a phase composition of 12%, 44% and 44% of CuO, Cu_2O and metallic Cu, respectively (Table 1). This is in agreement with the work described by ref. 13 that reports the conversion of $Cu(OH)_2$ into metallic Cu (35%) at 30 min of the reaction. The bulk composition differs from the surface at 30 min of the reaction as evident by XPS that shows the presence of 70% CuO and 30% copper in less than (II) oxidation state (Table 2). The latter could be a combination of both Cu(I) and metallic Cu as observed by Raman (shows the presence of Cu_2O, Fig. 5) and XANES (indicates the occurrence of metallic Cu, Fig. 4 and S2†), respectively. However, it is evident from spectroscopic data that the Cu-GDE is dominated by CuO, Cu_2O and $Cu(OH)_2$ at 30 min of the eCO_2R reaction. Hence, the ethylene production (Fig. 2 and 3) can still be mainly attributed to these oxides and hydroxide species (Fig. 4–6 and Tables 1 and 2), consistent with previous studies.[13] Although the role of metallic Cu in ethylene formation is not clear at this stage, a synergy between the copper oxides, hydroxide and metallic Cu may be necessary to produce ethylene at 30 min of the reaction.

At 60 min of the reaction, the phase transition is complete, and metallic Cu is established as evident from XANES (Fig. 4B), in excellent agreement with the work of Hung *et al.*[13] The LCA shows that the bulk composition consists mainly of metallic Cu (77%), but remarkably also includes 23% copper in the (II) oxidation state (Fig. S2† and Table 1). Even more interestingly, the surface composition does not contain any detectable copper in the (II) oxidation state as evident from XPS, corroborating the data observed at 30 min of the reaction, which indicated that the surface composition evolves differently from that of the bulk. Raman data show the presence of the CuO, Cu_2O, $Cu(OH)_2$ phases, along with CO adsorbed on metallic Cu (Fig. 5). This is consistent with XANES data (Fig. 4 and S2† and Table 1), and confirms that the bulk composition is indeed different from the surface composition as observed by XPS (Fig. 6 and Table 2). Careful assessment of the data reveal that the dynamic evolution of copper species during 60 min eCO_2R involve inter conversion of Cu(II) into metallic Cu and *vice versa*. The inter conversion may take place *via* intermediate species, such as Cu(I) detected at 30 min of the reaction. The presence of the copper oxide species, along with a dominant metallic Cu at 60 min, is consistent with the study that reported the presence of the $Cu(OH)_2$ and Cu_2O species along with metallic Cu in Cu-KOH and Cu-black electrodes.[15] The former contains 37.7% of $Cu(OH)_2$ and 25% of Cu_2O, while these species are in small amounts in the Cu-black electrode. However, these copper hydroxide and oxide species are shown to be present near the surface region of the electrodes, which is different from our findings that show them to be in

the bulk composition. The differences between the two Cu-KOH and Cu-black electrodes[15] and the present study can be attributed to the nature of the initial Cu-GDE compositions, which could also explain why no detectable copper oxide species are found in other studies that employ metallic Cu films.[12–14] Therefore, direct comparison between the studies may be difficult and it is clear that more *in situ* and *operando* spectroscopic studies are needed under commercially relevant eCO_2R conditions.

Interestingly, there is no correlation (Fig. 7) between the surface composition derived from XPS (Fig. 6 and Table 2) and the FE of ethylene (Fig. 2 and 3), as the steady state production of ethylene is evident even when the Cu-GDE surface contains either mainly copper oxides at 20 min of the reaction or only metallic Cu at 60 min (Fig. 7). This suggests that the bulk composition may be crucial for the C_{2+} production, rather than surface composition alone.[13,15] The argument gains strength with the data that show the presence of copper oxide and hydroxide phases with Cu(II) oxidation state as a common denominator, especially in the bulk composition at 20, 30 and 60 min, that indeed correlate very well with the ethylene production (Fig. 7). This finding is in line with an earlier *operando* XAS study that suggests a synergistic effect between the $Cu(OH)_2$ and Cu_2O species, along with the dominating metallic Cu species in Cu-KOH and Cu-black electrodes, improves the ethylene formation.[15]

The Cu(II) species in the bulk of Cu-GDE that contains metallic Cu as a major constituent in the present study. It also aligns well with theoretical studies that predict a key role of subsurface copper oxides in the C_{2+} production.[32,33]

The role of metallic Cu in ethylene production is not clear in the present study due to the coexistence of different copper oxides, hydroxide and metallic Cu phases during the reaction. However, we can assume that the metallic Cu could either facilitate CO_2 activation or adsorb activated CO_2 (perhaps as CO* intermediate as evident from Raman). The former could promote the reaction, while the latter could block/poison the Cu surface sites to some extent (under the reaction conditions). Hence, to some degree, it could hinder the C_{2+} formation. We note that the formation of metallic Cu and H_2 evolution rate go hand in hand. H_2 evolution kicks in at and above 30 min by when metallic Cu is established (see Fig. 3–6 and Tables 1 and 2), which coincide with a drop in CO and ethylene formation rates (see Fig. 3). Therefore, it appears that the metallic Cu promotes H_2 evolution rather than the ethylene formation under these experimental conditions. Interestingly, Raman shows CO adsorbed on the metallic Cu only at 60 min of the reaction by which time metallic Cu is well established (Fig. 4–6 and Tables 1 and 2). In turn, this may suggest that the CO_2 conversion mechanism in the presence of only copper oxides and hydroxide at 20 min of the reaction could be potentially different from the mechanism in the presence of majority of metallic Cu at 60 min.[44] The conversion mechanism requires further studies by suitable vibrational spectroscopic techniques and computational tools.

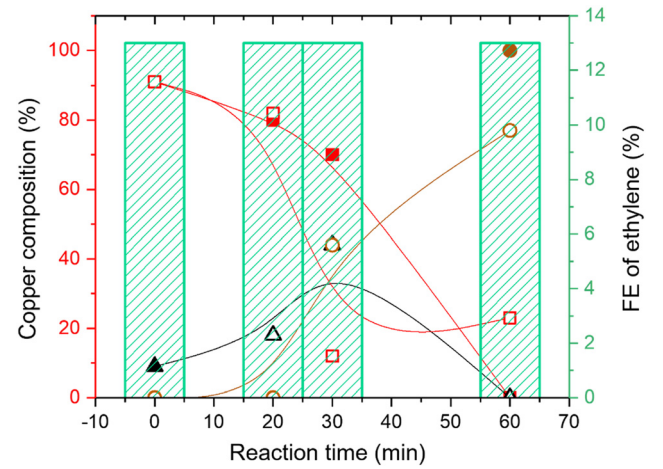

Fig. 7 Correlation between the copper composition (Tables 1 and 2) and FE of ethylene (Fig. 3) as a function of the reaction time. The open and filled symbols reflect the bulk composition derived from *in situ* XANES and surface composition deduced from quasi *in situ* XPS, respectively. Copper composition: Cu(II) (■; □), Cu(I) (▲; Δ), and Cu^0 (●; ○).

5. Summary and conclusions

A novel *operando* X-ray absorption spectroscopy (XAS) gas diffusion electrode (GDE) flow cell has been designed and fabricated. The applicability and versatility of the cell was demonstrated by conducting electrochemical CO_2 reduction (eCO_2R) over copper (Cu) GDE. XAS spectra at the Cu K-edge were measured in a transmission mode during the eCO_2R reaction for 60 min. The dynamic behaviour of copper during the reaction was captured by X-ray absorption near edge structure (XANES) spectra. Within the first 20 min of the reaction, copper is in oxidised state, as evident from linear combination analyses (LCA) of XANES and quasi *in situ* Raman spectroscopy and X-ray photoelectron spectroscopy (XPS). The majority of copper oxides reduced to metallic Cu (77%) after 60 min of the reaction; remarkably, however, 23% of copper is still in Cu(II) oxidation state, which is consistent with the quasi *in situ* Raman data that show the presence of copper oxides and $Cu(OH)_2$, along with CO adsorbed metallic Cu. In a marked contrast, the quasi *in situ* XPS shows 100% copper in <(II) oxidation state at 60 min, suggesting that the surface composition is different from the bulk composition. The complementary techniques enabled us to draw the following main conclusions:

1. Copper oxides (including CuO, Cu_2O) and hydroxide $Cu(OH)_2$ are responsible for the ethylene production, as evident from the first 20 min of the reaction.

2. A synergy between the metallic Cu and copper oxides and hydroxide that are present within the bulk composition of the catalyst cannot be ruled out in the promotion of ethylene production, as manifested at 30 and 60 min of the reaction.

3. Metallic Cu appears to promote hydrogen evolution, as evident from a correlation between the complementary quantitative spectroscopic and eCO_2R data.

Finally, our results demonstrate that a careful selection of complementary techniques to probe the catalyst composition from bulk to the surface is essential to deal with complex systems like Cu-GDE involving three phase reaction conditions.

Data availability

Data supporting the article are included in the main text and ESI.†

Author contributions

All authors have contributed to the work reported in this paper, and to the preparation of the manuscript.

Conflicts of interest

There are no conflicts of interest to declare.

Acknowledgements

The UK Catalysis Hub is kindly acknowledged for the resources and support provided *via* our membership of the UK Catalysis Hub Consortium, and funded by EPSRC grant no. EP/R026939/1, EP/R026815/1, EP/R026645/1, and EP/R027129/1. The authors also acknowledge support from the UKRI National Interdisciplinary Circular Chemical Economy Centre (EP/V011863/1). We thank the Diamond Light Source at the STFC Rutherford Appleton Laboratory for granting access to B18 beamline facilities through the Catalysis hub BAG. We are also grateful to the HarwellXPS centre for XPS and Raman studies. EPSRC North East Energy Materials Centre (NECEM), EP/R021503/1. We thank James Finn for providing a basic CAD image of the *operando* XAS GDE flow cell shown in Fig. 1.

References

1 S. Nitopi, E. Bertheussen and S. B. Scott, *et al.*, Progress and perspectives of electrochemical CO2 reduction on copper in aqueous electrolyte, *Chem. Rev.*, 2019, **119**, 7610–7672.
2 T. N. Nguyen and C. T. Dinh, Gas diffusion electrode design for electrochemical carbon dioxide reduction, *Chem. Soc. Rev.*, 2020, **49**, 7488–7504.
3 B. Endrodi, E. Kecsenovity, A. Samu, T. Halmagyi, S. Rojas-Carbonell, L. Wang, Y. Yan and C. Janaky, *Energy Environ. Sci.*, 2020, **13**, 4098–4105.
4 C.-T. Dinh, T. Burdyny, G. Kibria, A. Seifitokaldani, C. M. Gabardo, F. P. G. Arquer, A. Kiani, J. P. Edwards, P. Luna, O. S. Bushuyev, C. Zou, R. Quintero-Bermudez, Y. Pang, D. Sinton and E. H. Sargent, CO2 Electroreduction to Ethylene via Hydroxide-Mediated Catalysis at an Abrupt Reaction Interface, *Science*, 2018, **360**, 783–787.
5 D. Hursan and C. Janaky, *Chem. Commun.*, 2023, **59**, 1395–1414.
6 Y. Hori, A. Murata and R. Takahashi, *J. Chem. Soc., Faraday Trans.*, 1989, **1**(85), 2309–2326.
7 T. Burdyny and W. A. Smith, *Energy Environ. Sci.*, 2019, **12**, 1442–1453.
8 T. Haas, R. Krause, R. Weber, M. Demler and G. Schmid, *Nat. Catal.*, 2018, **1**, 32–39.
9 A. J. Martín, G. O. Larrazabal and J. Perez-Ramírez, *Green Chem.*, 2015, **17**, 5114–5130.
10 H. Xiang, S. Rasul, B. Hou, J. Portoles, P. Cumpson and E. H. Yu, *ACS Appl. Mater. Interfaces*, 2020, **12**, 601–608.
11 D. Higgins, C. Hahn, C. Xiang, T. F. Jaramillo and A. Z. Weber, *ACS Energy Lett.*, 2019, **4**, 317–324.
12 N. J. Firet, T. Burdyny, N. T. Nesbitt, S. Chandrashekar, A. Longo and W. A. Smith, *Catal. Sci. Technol.*, 2020, **10**, 5870–5885.
13 S.-F. Hung, F.-Y. Wu, Y.-H. Lu, T.-J. Lee, H.-J. Tsai, P.-H. Chen, Z.-Y. Lin, G.-L. Chen, W.-Y. Huang and W.-J. Zeng, *Catal. Sci. Technol.*, 2022, **12**, 2739–2743.
14 S. H. Lee, J. C. Lin, M. Farmand, A. T. Landers, J. T. Feaster, J. E. A. Acosta, J. W. Beeman, Y. Ye, J. Yano, A. Mehta, R. C. Davis, T. F. Jaramillo, C. Hahn and W. S. Drisdell, *J. Am. Chem. Soc.*, 2021, **143**, 588–592.
15 W. H. Lee, C. Lim, S. Y. Lee, K. H. Chae, C. H. Choi, U. Lee, B. K. Min, Y. J. Hwang and H.-S. Oh, *Nano Energy*, 2021, **84**, 105859.
16 J. M. Thomas, C. R. A. Catlow and G. Sankar, *Chem. Commun.*, 2002, 2921–2925.
17 M. A. Newton and W. van Beek, *Chem. Soc. Rev.*, 2010, **39**, 4845–4863.
18 S. K. Matam, M. H. Aguirre and A. Weidenkaff, *et al.*, *J. Phys. Chem. C*, 2010, **114**, 9439–9443.
19 B. Venezia, E. Cao, S. K. Matam, C. Waldron, G. Cibin, E. K. Gibson, S. Golunski, P. Wells, I. Silverwood, C. R. A. Catlow, G. Shankar and A. Gavriilidis, *Catal. Sci. Technol.*, 2020, **10**, 7842–7856.
20 P. K. Sharma, S. Rasul, D. Li and E. H. Yu, *Mater. Rep.: Energy*, 2023, **3**, 100196.
21 M. A. Isaacs, J. D. Jones, P. R. Davies, S. Guan, R. Lee, D. J. Morgan and R. Palgrave, *Mater. Chem. Front.*, 2021, **5**, 7931–7963.
22 S. Jiang, K. Klingan, C. Pasquini and H. Dau, *J. Chem. Phys.*, 2019, **150**, 041718.
23 A. J. Dent, G. Cibin, S. Ramos, S. A. Parry, D. Gianolio, A. D. Smith, S. M. Scott, L. Varandas, S. Patel, M. R. Pearson, L. Hudson, N. A. Krumpa, A. S. Marsch and P. E. Robbins, *J. Phys.: Conf. Ser.*, 2013, **430**, 012023.
24 B. Ravel and M. Newville, *J. Synchrotron Radiat.*, 2005, **12**, 537–541.
25 N. Fairley, V. Fernandez, M. Richard-Plouet, C. Guillot-Deudon, J. Walton, E. Smith, D. Flahaut, M. Greiner, M. Biesinger, S. Tougaard, D. Morgan and J. Baltrusaitis, *Appl. Surf. Sci. Adv.*, 2021, **5**, 100112.
26 S. Guan, P. R. Davies, E. K. Gibson, D. Lennon, G. E. Rossi, J. M. Winfield, J. Callison, P. P. Wells and D. J. Willock, *Faraday Discuss.*, 2018, **208**, 67–85.
27 A. A. Guda, S. A. Guda, A. Martini, A. N. Kravtsova, A. Algasov, A. Bugaev, S. P. Kubrin, L. V. Guda, P. Sot, J. A. van

Bokhoven, C. Coperet and A. V. Soldatov, *npj Comput. Mater.*, 2021, **7**, 203.
28 R. Q. Zhang and J. S. McEwen, *J. Phys. Chem. Lett.*, 2018, **9**, 3035–3042.
29 V. Gombac, *et al.*, *J. Phys. Chem. A*, 2010, **114**, 3916–3925.
30 C. Lamberti, S. Bordiga, F. Bonino, C. Prestipino, G. Berlier, L. Capello, F. D'Acapito, F. X. L. Xamena and A. Zecchina, *Phys. Chem. Chem. Phys.*, 2003, **5**, 4502–4509.
31 C. Lamberti, C. Prestipino, F. Bonino, L. Capello, S. Bordiga, G. Spoto, A. Zecchina, S. D. Moreno, B. Cremaschi, M. Garilli, A. Marsella, D. Carmello, S. Vidotto and G. Leofanti, *Angew. Chem., Int. Ed.*, 2002, **41**, 2341–2344.
32 C. Liu, M. P. Lourenco, S. Hedstrom, F. Cavalca, O. Diaz-Morales, H. A. Duarte, A. Nilsson and L. G. M. Pettersson, *J. Phys. Chem. C*, 2017, **121**(45), 25010–25017.
33 M. Favaro, H. Xiao, T. Cheng, W. A. Goddard, J. Yano and E. J. Crumlin, *Proc. Natl. Acad. Sci. U. S. A.*, 2017, **114**, 6706–6711.
34 S. Jiang, K. Klingan, C. Pasquini and H. Dau, *J. Chem. Phys.*, 2019, **150**, 041718.
35 Y. Deng, A. D. Handoko, Y. Du, S. Xi and B. S. Yeo, *ACS Catal.*, 2016, **6**, 2473–2481.
36 J. C. Hamilton, J. C. Farmer and R. J. Anderson, *J. Electrochem. Soc.*, 1986, **133**, 739–745.
37 H. Y. H. Chan, C. G. Takoudis and M. J. Weaver, *J. Phys. Chem. B*, 1999, **103**, 357–365.
38 S. D. Solomon, S. A. Rukowsky, M. L. Mahon and E. M. Halpern, *J. Chem. Educ.*, 2011, **88**, 1694–1697.
39 S. K. Haldor, *Platinum Nickel Chromium deposits, Geology, Exploration and Reserve Base*, 2017, pp. 1–35.
40 G. Iijima, T. Inomata, H. Yamaguchi, M. Ito and H. Masuda, *ACS Catal.*, 2019, **9**, 6305–6319.
41 R. M. Aran-Ais, R. Rizo, P. Grosse, G. Algara-Siller, K. Dembele, M. Plodinec, T. Lunkenbein, S. W. Chee and B. R. Cuenya, *Nat. Commun.*, 2020, **11**, 3489.
42 P. Grosse, D. Gao, F. Scholten, I. Sinev, H. Mistry and B. R. Cuenya, *Angew. Chem.*, 2018, **130**, 6300–6305.
43 M. C. Biesinger, *Surf. Interface Anal.*, 2017, **49**, 1325–1334.
44 M. D. Higham, M. G. Quesne and C. R. A. Catlow, *Dalton Trans.*, 2020, **49**, 8478–8497.